RSC Advances

ROYAL SOCIETY OF CHEMISTRY

COMMUNICATION

View Article Online
View Journal | View Issue

Cite this: *RSC Adv.*, 2016, **6**, 31191

Received 19th February 2016
Accepted 14th March 2016

DOI: 10.1039/c6ra04501d

www.rsc.org/advances

Published on 16 3 2016. Downloaded by Griffith University on 2020-07-02 8:34:18.

Piezo-Hall effect in single crystal p-type 3C–SiC(100) thin film grown by low pressure chemical vapor deposition

Afzaal Qamar,*[a] H.-P. Phan,[a] Toan Dinh,[a] Li Wang,[a] Sima Dimitrijev[ab] and Dzung Viet Dao[ab]

This article reports the first results on piezo-Hall effect in single crystal p-type 3C–SiC(100) Hall devices. Single crystal p-type 3C–SiC(100) was grown by low pressure chemical vapor deposition, and Hall devices were fabricated using the conventional photolithography and dry etching processes. An experimental setup capable of applying stress during Hall-effect measurements was designed to measure the piezo-Hall effect. The piezo-Hall effect is quantified by directly observing the variation in magnetic field sensitivity of the Hall devices upon an applied stress. The piezo-Hall coefficient P_{12} characterized by these measurements is found to be 6.4×10^{-11} Pa^{-1}.

The piezo-Hall effect in silicon (Si) has been widely studied over the past few decades and it has been used to compensate the magnetic field sensitivity drifts in Hall devices. The drift in magnetic field sensitivity of Hall devices results from several fabrication and post fabrication factors, with stresses introduced by encapsulation being the most important factor.[1–7] These stress variations can seriously affect the magnetic field sensing measurements and signal processing on chip by affecting the design parameters, temperature behavior and offset voltage.[1] The piezoresistive effect and piezo-Hall effect both are important for magnetic field sensors and a large number of studies on Si can be found in the literature.[1–7] However, the low energy band gap of Si limits its use for high temperature applications. Silicon carbide on the other hand has a wide band gap, high thermal conductivity, low thermal-expansion coefficient, better mechanical strength, good thermal-shock resistance and chemical stability, which make it a promising material for applications in harsh environments.[8–10] SiC can be found in various polytypes, including 4H–SiC, 6H–SiC, and 3C–SiC. The compatibility of 3C–SiC with the existing process of micro-electro-mechanical systems (MEMS) makes it a favorable polytype over other polytypes. Its hetero-epitaxial growth capability over Si substrates of different crystal orientations, *e.g.*, (100), (110) or (111),[11–13] make it a material of choice for harsh environment applications.

Various polytypes of SiC have been explored for piezoresistive effects and it has been found that the SiC is a promising material for strain or stress sensing applications in harsh environments.[14–20] Phan *et al.*[21–24] presented a comprehensive study on the piezoresistive effect in single crystal p-type 3C–SiC grown by low pressure chemical vapor deposition (LPCVD). A gauge factor (GF) upto 30 has been reported in p-type 3C–SiC which shows its potential for stress sensing applications. Fundamental piezoresistive coefficients of p-type 3C–SiC have also been reported. It has been found that the piezoresistive effect depends upon the crystal orientation and it can also be affected by the defect density in the crystal.[21–24] Piezojunction effects in p-3C–SiC/p-Si and n-3C–SiC/p-Si heterojunctions has also been reported, which shows that the applied stress can vary the current–voltage characteristics of the heterojunctions.[25,26] The pseudo-Hall effect (variation of offset voltage of Hall devices with applied stress without magnetic field) in LPCVD grown p-type 3C–SiC(100) and p-type 3C–SiC(111) Hall devices has been reported.[27–30] The offset voltage of the Hall devices varies significantly even without application of the magnetic field. This pseudo-Hall effect also depends upon the device geometry and crystal orientation and it can be minimized for certain crystallographic orientations. The pseudo-Hall effect is also important for magnetic field sensors because this effect must be subtracted in order to get the real magnetic field sensitivity of the Hall device.

To the best of our knowledge, there has been no report on the piezo-Hall effect in single crystal p-type 3C–SiC(100) Hall devices. Therefore, this paper aims to investigate the piezo-Hall effect in single crystal p-type 3C–SiC(100) Hall devices grown by LPCVD. The results achieved in this study can be used to understand the stress related drifts in the magnetic field sensitivity of Hall devices.

The growth of 3C–SiC thin film on Si(100) was performed using the LPCVD process at low temperature (1000 °C) utilizing

[a]*Queensland Micro- and Nanotechnology Centre, Griffith University, Queensland, Australia. E-mail: afzaal.qamar@griffithuni.edu.au*

[b]*School of Engineering, Griffith University, Queensland, Australia*

This journal is © The Royal Society of Chemistry 2016

Published on 16 3 2016. Downloaded by Griffith University on 2020-07-02 8:34:18.

SiH_4 and C_3H_6 precursors as the source of Si and C atoms.[31] Alternating supply epitaxy (ASE) was employed to grow the single crystal, 3C–SiC(100), on Si(100). The grown film was *in situ* doped with trimethyaluminium (TMAl) as a source of Al (p-type dopant).[31,32] The thickness of the grown film (300 nm) was measured by using a spectrophotometer Nanospec AFT 210. Physical characterization of the thin film was carried out by X-ray diffraction (XRD) and selected area electron diffraction (SAED) techniques. Fig. 1(a) shows the XRD pattern of the grown film in conventional θ–2θ scan mode. It can be confirmed from Fig. 1(a) that the single crystal 3C–SiC(100) was grown on Si(100). The inset of Fig. 1(a) shows the rocking curve of the 3C–SiC(100) peak and the observed FWHM value is 0.80°. Fig. 1(b) shows the SAED pattern of the grown thin film which confirms it is single crystalline. Atomic force microscopy (AFM) was used to measure the roughness of the grown thin film (Fig. 1(c)) which showed a root mean square (RMS) roughness of 20 ± 0.5 nm for a scan area of 5×5 μm. The electrical properties of the grown film were characterized using Hall effect measurements. The carrier concentration of p-type single crystalline 3C–SiC was found to be 8×10^{18} cm^{-3}, while the carrier concentration of the Si substrate was 5×10^{14} cm^{-3}. The resistivity of the SiC thin film was measured to be 0.44 Ω cm and the hole mobility of the single crystalline 3C–SiC thin film was found to be 1.88 cm^2 V^{-1} s^{-1}.

Rectangular Hall devices (700×300 μm) were fabricated by conventional photolithography and dry etch processes (Fig. 2(a)) to investigate the stress-induced piezo-Hall effect. The sputtering process was used to deposit aluminium for ohmic contacts to the device. After fabrication of the device, gold wire bonding was used for input and output signals from the device. The wafer was diced into strips with dimensions of $60 \times 9 \times 0.625$ mm to apply stress by the bending beam method. A dedicated experimental setup capable of applying magnetic field and mechanical stress simultaneously was designed to measure the piezo-Hall effect as shown in Fig. 2(b). Two permanent magnets having a field strength of 0.67 T with opposite poles were fixed in an aluminium box, leaving a space to insert the sample in the magnetic field between them. A cantilever was designed within the box in which one end of the beam with the devices was fixed, while the other end was bent by a known force in the presence of a magnetic field. The bi-layer model has been used to calculate the stress-induced to 3C–SiC Hall devices on Si beam. The method to numerically calculate the stress-induced into the 3C–SiC layer on Si strip is reported elsewhere.[23] The applied stress induced in the SiC layer was in the range of 0 to 343 MPa. The ohmic contacts were confirmed by *I*–*V* measurements as depicted in Fig. 2(c). Horizontal and vertical current leakage from 3C–SiC(100) through to

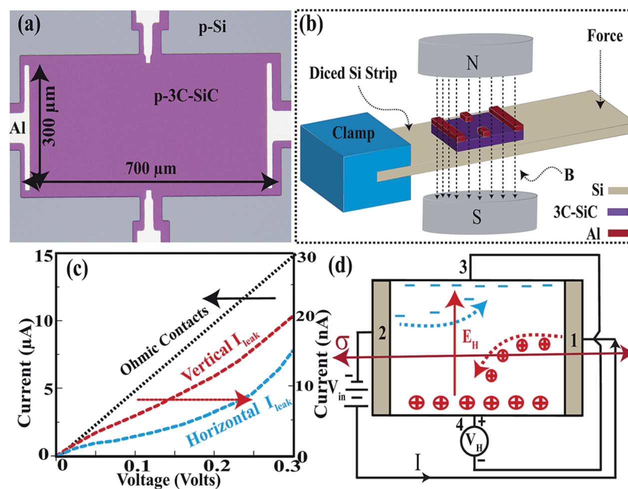

Fig. 2 (a) Microscopic image of the fabricated rectangular Hall device; (b) experimental setup for piezo-Hall measurements; (c) ohmic behavior of the contacts and leakage currents; (d) schematic presentation of the Hall effect in the fabricated device.

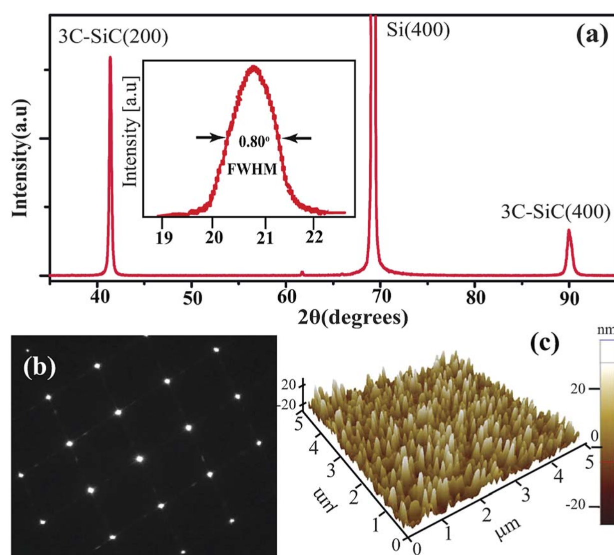

Fig. 1 (a) The XRD pattern of 3C–SiC(100) grown on Si(100), the inset shows the rocking curve; (b) SAED image of the thin film; (c) AFM image of 5×5 μm area of grown thin film.

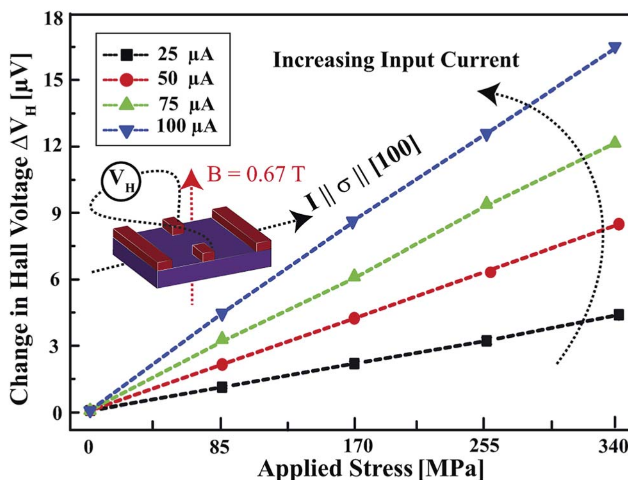

Fig. 3 Dependence of change in Hall voltage on applied stress at different input currents to the Hall device. The directions of applied magnetic field *B*, input current and applied stress are also shown.

This journal is © The Royal Society of Chemistry 2016

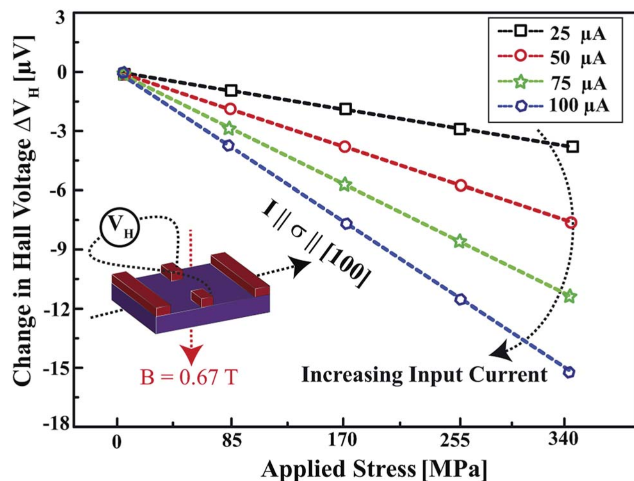

Fig. 4 Dependence of change in Hall voltage on applied stress at different input currents with magnetic field B reversed. The directions of magnetic field B, input current and applied stress are also shown.

the Si substrate (Fig. 2(c)) were also investigated to confirm that the leakage does not contribute to the measurements. The Al contacts showed good ohmic behavior and the total leakage of current was less than 0.5% of the total device current. A large valence band offset between p-Si and p-3C–SiC (1.7 eV) prevents the leakage current going through the SiC/Si junction.[25,26] A schematic presentation of the Hall effect in the fabricated device is shown in Fig. 2(d). The input current is applied between terminals 1 and 2 and the Hall voltage is observed at terminals 3 and 4. The contacts for current flow are strip-like in order to have the uniform current flow in the structure and the uniform effect of stress on the current flow. If the contacts for current are point-like, the current lines will bend and introduce a small source of error in the measurements. In the presence of a constant magnetic field, B, when stress is applied to the device at constant input current, the Hall voltage across terminals 3 and 4 will change with the increase of applied stress, which is the piezo-Hall effect.

For a cubic crystal such as 3C–SiC, the magnetic field B, current density J and the electric field vector E can be represented by the following equation:[1]

$$E = \rho J - (RB) \times J \tag{1}$$

where the coefficient ρ is resistivity and R is the Hall coefficient. The first term in eqn (1) describes the resistance while the second term describes the Hall effect. The coefficients ρ and R are generally second rank tensors, which reduce to simple scalars ρ_0 and R_0 in an unstressed case. The most general linear dependence of Hall coefficient R on the applied stress σ can be represented by the following equation:[1]

$$\frac{\Delta R_{ij}}{R_0} = \sum_{j} P_{ijkl}\sigma_{kl} \tag{2}$$

where P_{ijkl} is the piezo-Hall coefficient and σ_{kl} is the stress component. The directional indices i, j, k, and l can take values 1, 2, 3. The magnetic field sensitivity of the Hall device can be described by the following equation:[1]

$$S = V_H/I/B = R_H(G/t)[VA^{-1}T^{-1}] \tag{3}$$

where V_H is the Hall voltage observed at terminals 3 and 4, I is the current flowing through terminals 1 and 2 as shown in Fig. 2(d) and B is the magnetic field. R_H is the Hall coefficient, G is the geometrical correction factor and t is the thickness of the 3C–SiC thin film. Fig. 3 shows the variation of Hall voltage of the rectangular Hall plate when the stress is varied from 0 to 343 MPa. It can be observed from Fig. 3 that at a fixed value of current in the [100] direction, when stress is applied in the [100] direction, the Hall voltage increases linearly with the increase of applied stress. This increase of the Hall voltage at terminals 3 and 4 leads to a change in sensitivity of the Hall plate, *i.e.*, the piezo-Hall effect. As the value of the applied current is increased the corresponding Hall voltage is also increased and its stress dependency shows a smooth linear behavior. The offset voltage of the device, V_{off} (the voltage at terminals 3 and 4 in the absence of the magnetic field B), was also calculated and subtracted from the voltage measured at terminals 3 and 4 in order to get the true Hall voltage. Similarly, V_{off} also changes with stress and its variation with stress is also subtracted from the voltage measured at terminals 3 and 4 in order to get the true piezo-Hall effect which is different from the pseudo-Hall effect.[27–29]

Fig. 4 shows the variation of change in Hall voltage on the applied stress when the magnetic field B was reversed. It can be observed from Fig. 4 that the change in Hall voltage with applied stress showed reversed behavior as compared to the previous case. The Hall voltage V_H showed a linear decrease with the increase of applied stress, which verified the Hall effect measurements. The change in V_H is proportional to the change in applied current at terminals 1 and 2. The change in the sensitivity of Hall plates was measured by calculating the change in Hall voltage while ignoring the small variations in the dimensions of the Hall plate and very small variations in Hall angle due to deflection of the beam. Fig. 5 shows the

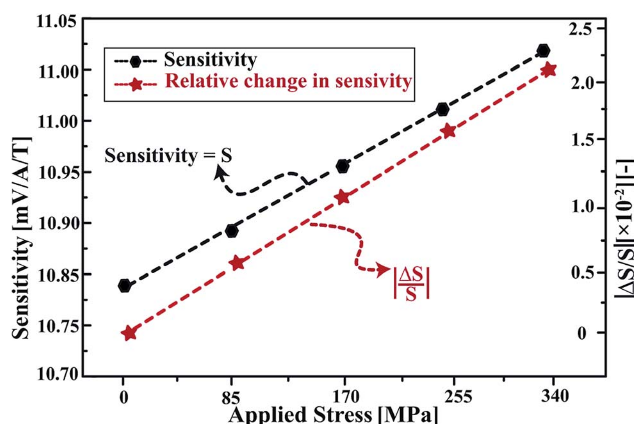

Fig. 5 The dependence of magnetic field sensitivity and the relative magnetic field sensitivity on the applied stress.

Published on 16 3 2016. Downloaded by Griffith University on 2020-07-02 8:34:18.

Published on 16 3 2016. Downloaded by Griffith University on 2020-07-02 8:34:18.

dependence of magnetic field sensitivity on the applied stress and the relative change in the magnetic field sensitivity. It can be observed that the magnetic field sensitivity linearly depends upon the applied stress and the maximum relative change in sensitivity of the device is 2.18% at a maximum stress of 343 MPa.

When the stress is always applied within the plane of the Hall plate, *i.e.*, perpendicular to the magnetic field B, piezo-Hall coefficients P_{12} can be determined.[1] In the present experiment when $B_{\|[001]}$, $I_{\|[100]}$, the Hall field $E_{H\|[010]}$ and the uni-axial stress is $\sigma_{\|[100]}$, eqn (2) is reduced to the following relation:

$$\frac{\Delta R_{\mathrm{H}}}{R_{\mathrm{H}}} = P_{12}\sigma_{[100]}, \quad B \perp (I \parallel \sigma \parallel [100]) \tag{4}$$

where P_{12} is the piezo-Hall coefficient and $\sigma_{[100]}$ is the stress parallel to the [100] direction. The relation between change in magnetic field sensitivity and the piezo-Hall coefficient P_{12} is derived from eqn (3) and (4) and is given as:

$$P_{12} = \frac{\Delta S}{S} \times \frac{1}{\sigma} \tag{5}$$

where ΔS is the change in magnetic field sensitivity due to the applied stress. The piezo-Hall coefficient P_{12} calculated from the above relation was found to be 6.4×10^{-11} Pa^{-1}.

The piezo-Hall effect in LPCVD grown single crystal p-type 3C–SiC(100) thin film has been observed. After the fabrication of 3C–SiC(100) Hall plates, a dedicated setup capable of applying magnetic field and stress simultaneously has been designed to observe the piezo-Hall effect. Variations in Hall voltage with the application of applied stress have been used to record the variations in magnetic field sensitivities which is then used to calculate the piezo-Hall coefficient P_{12} having a value of 6.4×10^{-11} Pa^{-1}. Variations upto 2.18% in relative magnetic field sensitivity of the fabricated Hall plates were easily observed with the designed setup at the maximum applied stress of 343 MPa. The results of this study can be utilized to compensate for the piezo-Hall effect in the design of p-type 3C–SiC(100) Hall sensors.

Acknowledgements

This work was performed in part at the Queensland node of the Australian National Fabrication Facility, a company established under the National Collaborative Research Infrastructure Strategy to provide nano and micro-fabrication facilities for Australia's researchers. This work has been partially supported by the Griffith University's New Researcher Grants.

References

1 B. Halg, *J. Appl. Phys.*, 1988, **64**, 276–282.
2 S. Huber, C. Schott and O. Paul, *IEEE Sens. J.*, 2013, **13**, 2890–2898.
3 H. Husstedt, U. Ausserlechner and M. Kaltenbacher, *IEEE Sens. J.*, 2011, **11**, 2993–3000.
4 A. Nathan and T. Manku, *Appl. Phys. Lett.*, 1993, **62**, 2947–2949.
5 J. M. Cesaretti, W. P. Taylor, G. Monreal and O. Brand, *IEEE Trans. Magn.*, 2009, **45**, 4482–4485.
6 R. Steiner, C. Maier, M. Mayer, S. Bellekom, H. Baltes and J. Mems, *IEEE*, 1999, **8**, 466–472.
7 D. Manic, J. Petr and R. Popovic, *Microelectron. Reliab.*, 2001, **41**, 767–771.
8 P. M. Sarro, *Sens. Actuators, A*, 2000, **82**, 210–2018.
9 G. yi Li, J. Ma, G. Peng, W. Chen, Z. yong Chu, Y. he Li, T. jiao Hu and X. dong Li, *ACS Appl. Mater. Interfaces*, 2014, **6**, 22673–22679.
10 M. Mehregany, C. A. Zorman, N. Rajan and C. H. Wu, *Proc. IEEE*, 1998, **86**, 1594.
11 J. S. Shor, D. Goldstein and A. D. Kurtz, *IEEE Trans. Electron Devices*, 1993, **40**, 1093.
12 F. L. Via, M. Camarda and A. L. Magna, *Appl. Phys. Rev.*, 2014, **1**, 031301.
13 S. Roy, C. Jacob and S. Basu, *IEEE Trans. Electron Devices*, 2003, **94**, 298.
14 J. Casady and R. Johnson, *Solid-State Electron.*, 1996, **39**, 1409–1422.
15 J. Bi, G. Wei, L. Wang, F. Gao, J. Zheng, B. Tang and W. Yang, *J. Mater. Chem. C*, 2013, **1**, 4514.
16 F. Gao, J. Zheng, M. Wang, G. Wei and W. Yang, *Chem. Commun.*, 2011, **47**, 11993.
17 R. Shao, K. Zheng, Y. Zhang, Y. Li, Z. Zhang and X. Han, *Appl. Phys. Lett.*, 2012, **101**, 233109.
18 T. Akiyama, D. Briand and N. F. Rooij, *J. Micromech. Microeng.*, 2012, **22**, 085034.
19 R. S. Okojie, A. A. Ned, A. D. Kurtz and W. N. Carr, *IEEE Trans. Electron Devices*, 1998, **45**, 785.
20 R. Okojie, D. Lukco, V. Nguyen and E. Savrun, *IEEE Electron Device Lett.*, 2015, **36**, 174.
21 H. P. Phan, P. Tanner, D. V. Dao, L. Wang, N. T. Nguyen, Y. Zhu and S. Dimitrijev, *IEEE Electron Device Lett.*, 2014, **35**, 399–401.
22 H. P. Phan, D. V. Dao, P. Tanner, N. T. Nguyen, L. Wang, Y. Zhu and S. Dimitrijev, *Appl. Phys. Lett.*, 2014, **104**, 111905.
23 H. P. Phan, D. V. Dao, P. Tanner, N. T. Nguyen, J. S. Han, S. Dimitrijev, G. Walker, L. Wang and Y. Zhu, *J. Matter. Chem. C*, 2014, **2**, 7176–7179.
24 H. P. Phan, D. V. Dao, L. Wang, T. Dinh, N.-T. Nguyen, A. Qamar, P. Tanner, S. Dimitrijev and Y. Zhu, *J. Matter. Chem. C*, 2015, **3**, 1172–1176.
25 A. Qamar, P. Tanner, D. V. Dao, H.-P. Phan and T. Dinh, *IEEE Electron Device Lett.*, 2014, **35**, 1293–1295.
26 A. Qamar, D. V. Dao, P. Tanner, H.-P. Phan, T. Dinh and S. Dimitrijev, *Appl. Phys. Express*, 2015, **8**, 061302.
27 A. Qamar, H.-P. Phan, D. Dao, P. Tanner, T. Dinh, L. Wang and S. Dimitrijev, *IEEE Electron Device Lett.*, 2015, **36**, 708–710.
28 A. Qamar, P. Hoang-Phuong, J. Han, P. Tanner, T. Dinh, L. Wang, D. V. Dao and S. Dimitrijev, *J. Mater. Chem. C*, 2015, **3**, 8804–8809.
29 A. Qamar, P. Hoang-Phuong, J. Han, P. Tanner, T. Dinh, L. Wang, D. V. Dao and S. Dimitrijev, *J. Mater. Chem. C*, 2015, **3**, 8804–8809.

 This journal is © The Royal Society of Chemistry 2016

30 P. Hoang-Phuong, A. Qamar, D. V. Dao, T. Dinh, L. Wang, J. Han, P. Tanner, S. Dimitrijev and N.-T. Nguyen, *RSC Adv.*, 2015, **5**, 56377–56381.
31 L. Wang, A. Iacopi, S. Dimitrijev, G. Walker, A. Fernandes, L. Hold and J. Chaia, *Thin Solid Films*, 2014, **564**, 39–44.
32 L. Wang, S. Dimitrijev, J. Han, P. Tanner, A. Lacopi and L. Hold, *J. Cryst. Growth*, 2011, **329**, 67–70.

Published on 16 3 2016. Downloaded by Griffith University on 2020-07-02 8:34:18.